Simultaneous enhancement in charge separation and onset potential for water oxidation in a BiVO4 photoanode by W – Ti codoping

Zhao, Xin; Hu, Jun; Wu, Bo; Banerjee, Amitava; Chakraborty, Sudip; Feng, Jianyong; Zhao, Zongyan; Chen, Shi; Ahuja, Rajeev; Sum, Tze Chien; Chen, Zhong

2018

Zhao, X., Hu, J., Wu, B., Banerjee, A., Chakraborty, S., Feng, J., . . . Chen, Z. (2018). Simultaneous enhancement in charge separation and onset potential for water oxidation in a BiVO4 photoanode by W – Ti codoping. Journal of Materials Chemistry A, 6(35), 16965-16974. doi:10.1039/C8TA05491F

https://hdl.handle.net/10356/81164

https://doi.org/10.1039/C8TA05491F

Simultaneous enhancement in charge separation and onset potential for water oxidation in $BiVO_4$ photoanode by W-Ti codoping

Xin Zhao,[a†] Jun Hu,[a,e†] Bo Wu,[b] Amitava Banerjee,[c] Sudip Chakraborty,[c]* Jianyong Feng,[a] Zongyan Zhao,[f] Shi Chen,[b] Rajeev Ahuja,[c,d] Tze Chien Sum,[b]* Zhong Chen[a]*

[a]*School of Materials Science and Engineering, Nanyang Technological University, 50 Nanyang Avenue, 639798, Singapore, Singapore.*

[b]*School of Physical and Mathematical Sciences, Nanyang Technological University, 637371, Singapore, Singapore*

[c]*Materials Theory Division, Department of Physics and Astronomy, Uppsala University, 75120, Sweden*

[d]*Applied Materials Physics, Department of Materials and Engineering, Royal Institute of Technology (KTH), S-100 44 Stockholm, Sweden*

[e]*School of Chemical Engineering, Northwest University, Xi'an, P. R. China 710069*

[f]*Faculty of Materials Science and Engineering, Kunming University of Science and Technology, Kunming 650093, P. R. China*

E-mail: ASZChen@ntu.edu.sg

Abstract: Efficient charge separation of photo-generated electrons and holes is critical to achieve high solar to hydrogen conversion efficiency in photoelectrochemical (PEC) water splitting. N-type doping is generally used to improve the conductivity by increasing the majority carrier's density and enhance the charge separation in the photoanode. However, minority carrier's transport is also very important in the process of charge separation, especially in materials that possess inadequate minority carrier mobility. Herein, we take $BiVO_4$ PEC water splitting cell as an example to demonstrate how to analyze the limiting factor, and to formulate the corresponding solutions to improve the hole mobility. The benefits and problems caused by n-type doping (W-doping here) of $BiVO_4$ are analyzed. Codoping with Ti further enhances the charge separation by improving the hole transport and leads to a cathodic shift of the photocurrent onset potential. A high charge separation efficiency (79% at 1.23 V_{RHE}) in a compact $BiVO_4$ photoanode has been achieved without any nanostructure formation. Theoretical results show that W-Ti codoping has decreased the hole polaron hopping activation energy by 11.5% compared with mono W doping, and this has resulted in hole mobility increase by 29%. The calculated adsorption energy and reaction Gibbs free energies indicate that the Ti site is energetically more favorable for water splitting. Moreover, Ti site possesses a lower overpotential in W-Ti codoped sample compared with mono W doped sample. The current study indicates that in order to improve the solar energy conversion efficiency, there should be a balanced charge transport of both majority and minority charge carriers. This can be achieved by simply choosing appropriate codoping elements.

1. Introduction

Solar is one of the most promising renewable and clean energy sources to overcome the environmental challenges caused by fossil fuel consumption. Photoelectrochemical solar water splitting is one of the most promising solutions to convert solar energy into clean chemical energy.[1-4] Efficient charge separation of photo-generated electrons and holes is critical to achieving high solar to hydrogen conversion efficiency. Doping is an effective way to improve the conductivity by increasing the majority carrier's density and enhance the charge separation.[5, 6] However, minority carrier's transport should not be neglected, especially for those having poor transport ability. In principle, a well-balanced electron and hole transport is crucial for high efficiency[7] , however, research in this area is still lacking.

Nanostructuring is known to be an effective strategy to shorten the carrier transport distance from where it is generated to the reaction surface, which could effectively reduce the photo-generated carriers' recombination.[6, 8-12] Heterojunction is another effective way to enhance the minority carrier's transport, using the internal electric field formed between the junction to facilitate the charge carrier separation.[13, 14] Gradient-doped structure, in which the surface doping concentration is lower than the bulk concentration, is also an effective way to promote the minority carrier to diffuse to the surface.[15, 16] However, these strategies do not change the mobility of minority carriers. Fundamental understanding of intrinsic minority transport is still lacking.

In addition to bulk charge separation, surface charge injection to oxidize water is also a key step to the energy conversion efficiency. Due to the sluggish oxygen evolution reaction and the presence of surface states, surface recombination is generally inevitable. Thus, these recombination losses lead to low charge transfer efficiency and high overpotential for PEC water oxidation. Numerous approaches including surface treatment or etching,[17-19] overlayer coating,[20-

[24] or electrocatalyst deposition[6, 25, 26] have been applied to effectively suppress the surface recombination. However, there is lack of understanding of the surface catalytic property of both pristine and doped $BiVO_4$ in the existing literature.

Here, we take $BiVO_4$ photoelectrochemical (PEC) water splitting cell as an example to demonstrate how to analyze the limitation factor for the energy conversion efficiency, as well as to formulate corresponding solutions to improving the charge separation. Codoping was employed here to overcome the limitations on the basis of the reported enhancement.[27-31] Surface catalytic property of pristine and doped $BiVO_4$ are analyzed from both experimental and theoretical perspectives. Monoclinic $BiVO_4$ is one of the most promising photoanodes for PEC water-splitting. Its 2.4 eV optical bandgap corresponds to a theoretical conversion efficiency of 9.1%. It also possesses a favorable conduction band edge position for water splitting.[6, 16, 32, 33] In previous reports, W or Mo doping was found to be effective in enhancing the electron conductivity.[34, 35] In this study, we quantitatively analyzed the limiting factor of $BiVO_4$ and pointed out both the benefit and deficiency caused by n-type doping (W-doping here). It is found that W doping increases the static dielectric constant which lowers the carrier mobility although it enhances the electron density. We found that W-Ti codoping into $BiVO_4$ can lower the static dielectric constant, which enhances the hole mobility and further improves the charge separation efficiency to 79%. Moreover, this codoping has also caused a cathodic shift of the photocurrent onset potential by introducing active surface sites related to the presence of Ti. An impressively high charge separation efficiency (79% at 1.23 V_{RHE}) and a simultaneous cathodic shift of the photocurrent onset potential has been realized by W-Ti codoping in a compact $BiVO_4$ photoanode without any nanostructure formation.

2. Experimental

Preparation of thin films: Bismuth trioxide, Ammonium metavanadate, ammonium tungstate hydrate and Titanium (IV) bis (ammonium lactato) dihydroxide solution were dissolved in ethylene glycol with proper amount of nitric acid (100 ml solution containing 5 ml nitric acid) to form 0.03 M Bi, V, W, and Ti precursor solutions respectively. These solutions were mixed according to stoichiometric ratio for W doped $BiVO_4$ and W-Ti codoped $BiVO_4$. Citric acid (CA) was also added according to stoichiometric ratio of CA:M=1.5:1 (M is the total amount of cation including dopants). After mixing, 70 µl of the precursor solution were dropped on the FTO substrates (1 cm × 2 cm with half of the length covered by transparent tape for electrical contact). The samples were dried at 120°C for 30 minutes, and subsequently calcined at 500 °C in a furnace for 30 min to obtain the thin films. The annealing temperature 500 °C was chosen according to the TG-DTA results (Fig. S1).

Co-Pi decorated W-Ti codoped $BiVO_4$ was performed by electrodeposition. An electrochemical cell with three-electrode configuration was employed for the CoPi electrodeposition. The Pt foil was used as counter electrode and Ag/AgCl (in saturated KCl solution) was used as the reference electrode. 0.5 mM $Co(NO_3)_2$ was added into 0.1M KPi solution to serve as the electrolyte, and the pH value was adjusted to 7. For the electrodeposition, constant current density of 20 µA/cm^2 was applied. The amount of CoPi was estimated to be 5 mC/cm^2. After electrodeposition, the films were washed with deionized water.

Characterization: The morphologies were observed using field emission scanning electron microscopy (FESEM, JEOL JSM-7600F). Crystallinity was identified by X-ray diffraction (XRD) patterns (Shimadzu 6000 X-ray diffractometer) with Cu Kα radiation (λ = 0.154 nm), using a 2θ scan mode with the fixed incidence angle at 1°. The light absorption was obtained by measuring the reflectance and transmittance using UV-visible spectrophotometer with an integrating sphere

(Lambda 750S, Perkin-Elmer). Differential thermal analysis and thermo-gravimetric analysis were conducted by a Netzsch thermal analyzer (STA 449 C). The chemical state of W and Ti were investigated by X-ray photoelectron spectroscopy (XPS, Omicron EA125). The binding energy was calibrated by C1s (284.6 eV). Raman spectra were obtained using a confocal Raman microscopy (Witec alpha300 SR) with laser wavelength of 488 nm. Elemental composition was analyzed by Energy-dispersive X-ray spectroscopy (EDS) equipped in a field-emission scanning electron microscopy with transmission electron detector (FESEM, JEOL JSM-7600F).

Photoelectrochemical measurements were performed using a three-electrode configuration (PCI4/300™ potentiostat with PHE200™ software, Gamry Electronic Instruments, Inc.), with a $BiVO_4$ working electrode, a Pt foil as a counter electrode and a reference electrode of Ag/AgCl. The light source for photoelectrochemical measurement is a solar simulator (HAL-320, Asahi Spectra Co., Ltd.) with power intensity 100 $mW \cdot cm^{-2}$ calibrated with a solar reference cell. The photocurrents of water oxidation were measured in 0.5 M Na_2SO_4 aqueous solution with a scan rate of 30 $mV \cdot s^{-1}$. The photocurrents tested with hole scavenger to obtain ~100% charge transfer efficiency was measured in 0.5 M Na_2SO_4 aqueous solution mixed with 0.1 M Na_2SO_3. The Mott-Schottky plots were carried out using an AUTOLAB Potentiostat-Galvanostat (AUTOLAB PGSTAT302 N) in 0.5 M Na_2SO_4 aqueous solution, and the frequency was set at 1 kHz according to reported works.[6, 36-38]

Transient absorption measurements were performed using commercial EOS™ setup in non-degenerate pump-probe configuration (Ultrafast Systems LLC). In the measurement, the pump and probe beams were incident on the sample with a small incident angle (< 10 °). The 400 nm pump pulses were generated from the second harmonic of the 800 nm laser beam using a barium

borate (BBO) crystal. The 800 nm laser beam was generated from a 1-kHz regenerative amplifier (Coherent Legend^{TM}, 150 fs, 1 mJ). A mode-lock Ti-sapphire oscillator (Coherent Vitesse, 80MHz) was used for the amplifier. The probe pulse was a white light continuum generated from a photonic fiber using a Nd:YAG laser (center wavelength: 1064 nm). A CMOS sensor was used to collect the probe light after passing through the samples and another one was used to collect the probe light before passing through the sample as the reference.

3. Results and discussion

3.1 Analysis of the limiting factor of $BiVO_4$ photoanode for PEC water oxidation

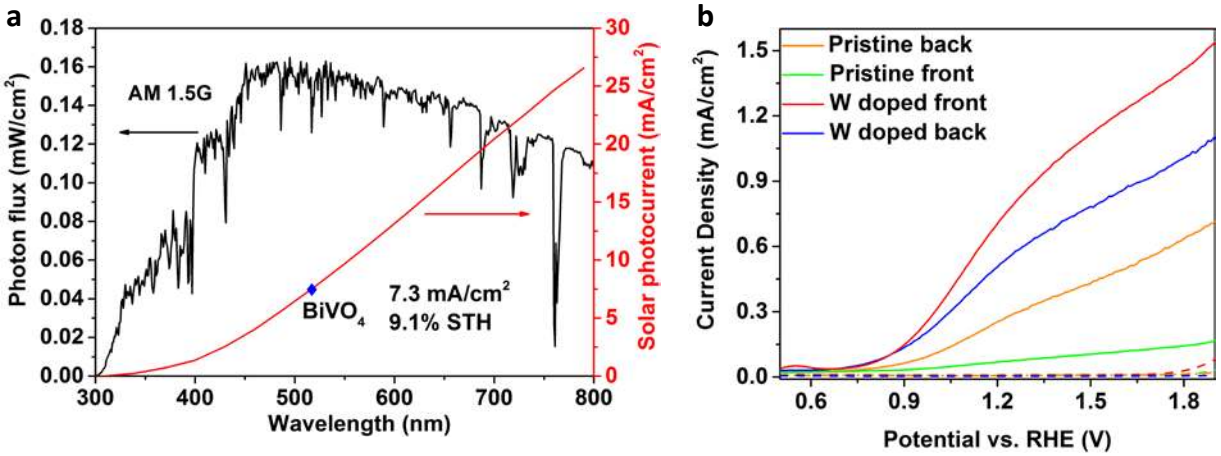

Fig. 1 (a) Dependence of theoretical solar photocurrent density of photoelectrodes under AM 1.5G irradiation (100 mW/cm^2). (b) Front and back side illumination photocurrents of pristine and W doped $BiVO_4$ under AM 1.5G irradiation (100 mW/cm^2). Dark currents were shown in dash lines.

Theoretical photocurrent of a photoelectrode under AM 1.5G irradiation (100 mW/cm^2) is shown in Fig. 1a, which is based on the assumption that 100% of the photons in the solar spectrum with energies beyond the bandgap is absorbed and converted.[3] Theoretical solar to hydrogen efficiency of $BiVO_4$ is 9.1%, corresponding to a photocurrent of about 7.3 mA/cm^2.[3] However,

as shown in Fig. 1b, the photocurrent of pristine $BiVO_4$ is only 0.27 mA/cm^2 at 1.23 V_{RHE}. To explore the reasons, each critical steps in a PEC water splitting process should be analyzed. The water oxidation photocurrent is determined by three factors as expressed by the following equation:[39]

$$J_{H_2O} = J_0 \times \eta_{abs} \times \eta_{sep} \times \eta_{inj} \quad (1)$$

where J_{H_2O} is the total water splitting photocurrent, J_0 is the theoretical solar photocurrent (7.3 mA/cm^2 for $BiVO_4$), η_{abs} is the light absorption efficiency, η_{sep} is the charge separation efficiency for photo-generated carriers, and η_{inj} is the interfacial charge transfer efficiency for water oxidization. When a hole scavenger is added into the electrolyte, the interfacial charge transfer efficiency can be assumed to be 100% (η_{inj}=1).[39] The photocurrent measured with the hole scavenger $J_{Na_2SO_3}$ in the electrolyte can be determined by equation 2: [39]

$$J_{Na_2SO_3} = J_0 \times \eta_{abs} \times \eta_{sep} = J_{abs} \times \eta_{sep} \quad (2)$$

where $J_{Na_2SO_3}$ is the oxidation photocurrent of Na_2SO_3, J_{abs} is the maximum photocurrent of a given photoanode based on its light absorption efficiency. The light absorption efficiency (η_{abs}) of pristine $BiVO_4$ with a thickness of around 190 nm is shown in Fig. S2. According to this light absorption efficiency, the J_{abs} is calculated to be 3.54 mA/cm^2. We also measured the oxidation photocurrent of Na_2SO_3 (Fig. S3). From equations 1 and 2, the obtained charge separation efficiency of the pristine $BiVO_4$ is 22%, while the interfacial charge transfer efficiency is 34% at 1.23 V_{RHE}. It is concluded that the charge separation is the limiting factor for the PEC performance.

Fig. 1b shows front (the electrolyte side) and back (the FTO side) side illumination photocurrents of pristine and W doped $BiVO_4$. Higher front illumination photocurrent indicates

better electron transport. Otherwise, higher back illumination photocurrent indicates better hole transport. (Details in supporting information). From Fig. 1b, the photocurrent under front side illumination is much lower than that of back side illumination, which indicates poor electron transport in pristine $BiVO_4$.[10] The poor electron conductivity is the main reason that limits the separation efficiency.

W doping was then employed in this study, and the photocurrent was enhanced significantly (Fig. 1b). The calculated η_{sep} and η_{inj} of W doped $BiVO_4$ at 1.23 V_{RHE} are 42% and 52% respectively. Although W doping greatly enhances both the charge separation (1.9-fold) and interfacial charge transfer (1.6-fold) efficiencies, the absolute photocurrent density is still low. Through W doping, the poor electron conductivity has been improved, however, the hole transport becomes a limit factor determining the performance, which is reflected from Fig. 1b that back photocurrent is smaller than front. In the following, we are going to improve the hole transport by codoping with Ti.

3.2 Effect of W-Ti codoping on the charge separation of $BiVO_4$

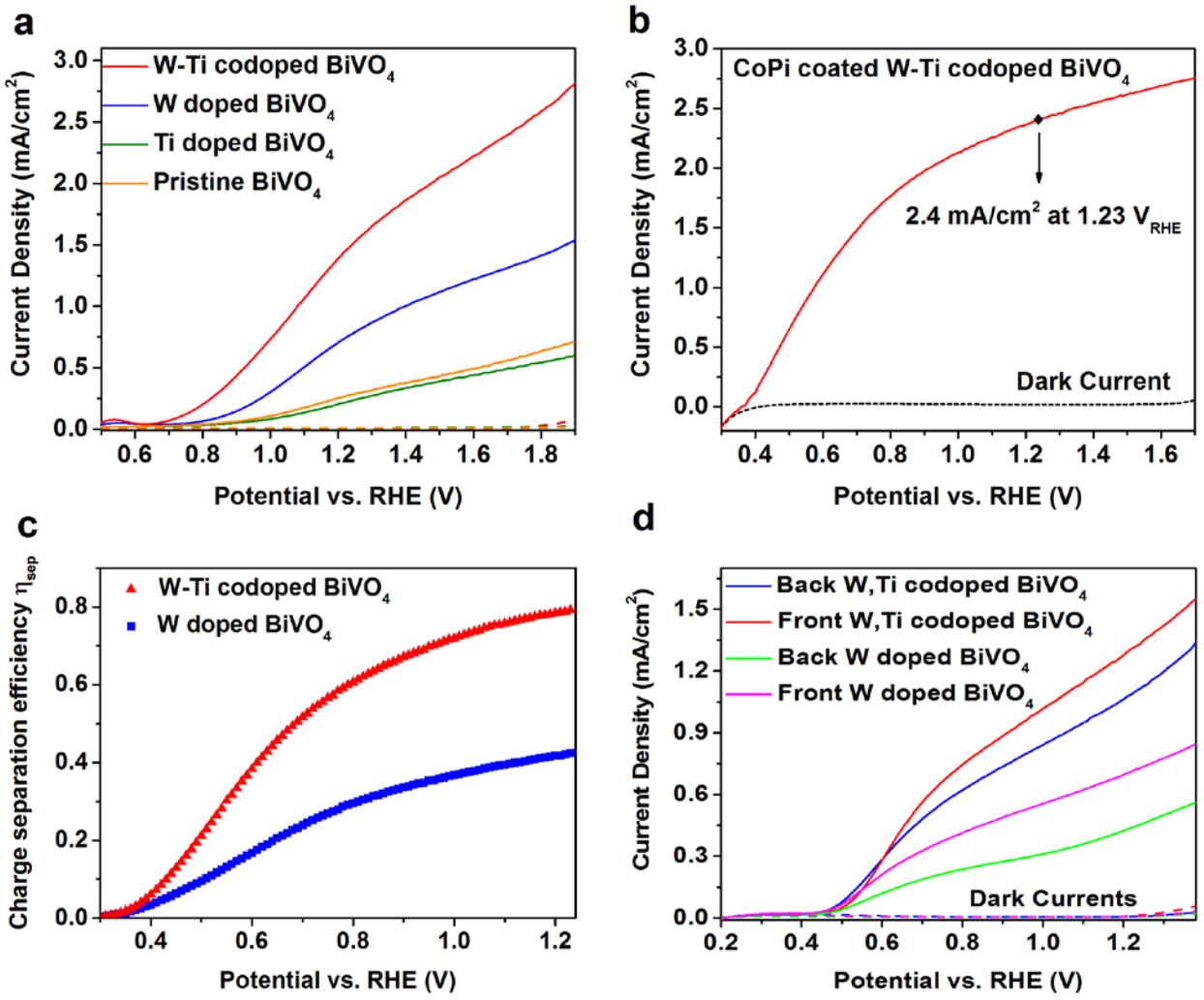

Fig. 2 (a) Photocurrents of W doped $BiVO_4$, Ti doped $BiVO_4$ and W-Ti codoped $BiVO_4$ films under 1 sun simulated AM1.5G illumination. Dark currents were shown in dash lines. (b) Photocurrent of W-Ti codoped $BiVO_4$ decorated with CoPi under 1 sun simulated AM1.5G illumination. Dark currents were shown in dash lines. (c) Charge separation efficiencies of W doped $BiVO_4$ and W-Ti codoped $BiVO_4$ as a function of applied potential. (d) Photocurrents of W doped $BiVO_4$ and W-Ti codoped $BiVO_4$ with the same thickness (≈170 nm) in 0.5 M Na_2SO_4 and 0.1 M Na_2SO_3 illuminated from front

side (electrolyte-$BiVO_4$ side) and back side (FTO-$BiVO_4$ side) with a 400 nm cut-off filter.

W-Ti codoped $BiVO_4$ films were prepared by drop-casting method reported before.[40] The crystallinity and evidence for successful doping was analyzed by XPS, EDX and Raman (Fig. S4-S7 and Table S1, details are given in the supporting information). We find that after Ti codoping into W doped $BiVO_4$, the performance can be greatly enhanced. After optimization (Fig. S8) of Ti codoping concentrations, a nominal 2%W and 2%Ti codoped $BiVO_4$ has much better performance than the W doped $BiVO_4$, corresponding to almost 2 times that of W doped $BiVO_4$ (Fig. 2a). For comparison, the photocurrents of Ti doped $BiVO_4$ is similar to the pristine sample. This indicates that Ti mono-doping has no effect on the photocurrent improvement. This is understandable since the electron conductivity is the limiting factor for pristine $BiVO_4$ and Ti doping has no contribution to this. Based on the series comparison, we conclude that to obtain high solar conversion efficiency, the electron conductivity has to be improved as the foundation, based on which further enhancement can be designed. Fig. 2b shows the photocurrent of CoPi decorated W-Ti codoped $BiVO_4$, in which CoPi is loaded by electro-deposition with the loading amount of around 5 mC/cm^2 according to a previous work.[41] The photocurrent reaches to 2.4 mA/cm^2 at 1.23 V_{RHE} by suppression of the surface recombination after the decoration of CoPi.

It has been shown that W-Ti codoping does not alter the morphology, film thickness (Fig. S9), and the light absorption efficiency (Fig. S10). We have also calculated the interfacial charge transfer efficiency η_{inj} of W doped $BiVO_4$ and W-Ti codoped $BiVO_4$ based on the

hole scavenger Na_2SO_3 oxidation photocurrent (Fig. S11). They are 52% and 54%, respectively. W-Ti codoping has resulted in a very small enhancement on the interfacial charge transfer. It is concluded that the great enhancement in the photocurrent by codoping Ti is mainly attributed to the better charge separation process rather than surface charge transfer. The calculated charge separation η_{sep} of W doped $BiVO_4$ and W-Ti codoped $BiVO_4$ obtained from equation 2 are shown in Fig. 2c. At 1.23 V_{RHE}, the η_{sep} of W codoped $BiVO_4$ is 42%, while that of W-Ti codoped $BiVO_4$ is 79%. Thus, Ti codoping has greatly enhanced the charge separation efficiency.

In order to understand how Ti codoping improves the charge separation efficiency, photocurrent of W doped $BiVO_4$ and W-Ti codoped $BiVO_4$ with the same thickness (≈170 nm) illuminated from front and back side was measured (Fig. 2d). In consideration of the fact that FTO has light absorption in the UV region (Fig. S12), which affects the light absorption of our photocatalysts by front and back illumination, we use the 400 nm cut-off filter to avoid the possible influence by FTO. To reflect the bulk transport property, hole scavenger Na_2SO_3 was added. As shown in Fig. 2d, the photocurrent at 1 V_{RHE} of W doped $BiVO_4$ from front illumination is 60% higher than that of from back illumination. This indicates a relatively poor hole transport property in W doped $BiVO_4$. However, this disparity is narrowed in the W-Ti codoped sample, in which the front side photocurrent is 21% higher than the back side. This implies that Ti codoping in W doped $BiVO_4$ has greatly improved the hole transport. Considering this method is a rough estimation on the electron and hole transport, transient absorption spectroscopy (TAS) is further employed to investigate the photophysics and carrier dynamics in the W doped and W-Ti co-doped $BiVO_4$ films.

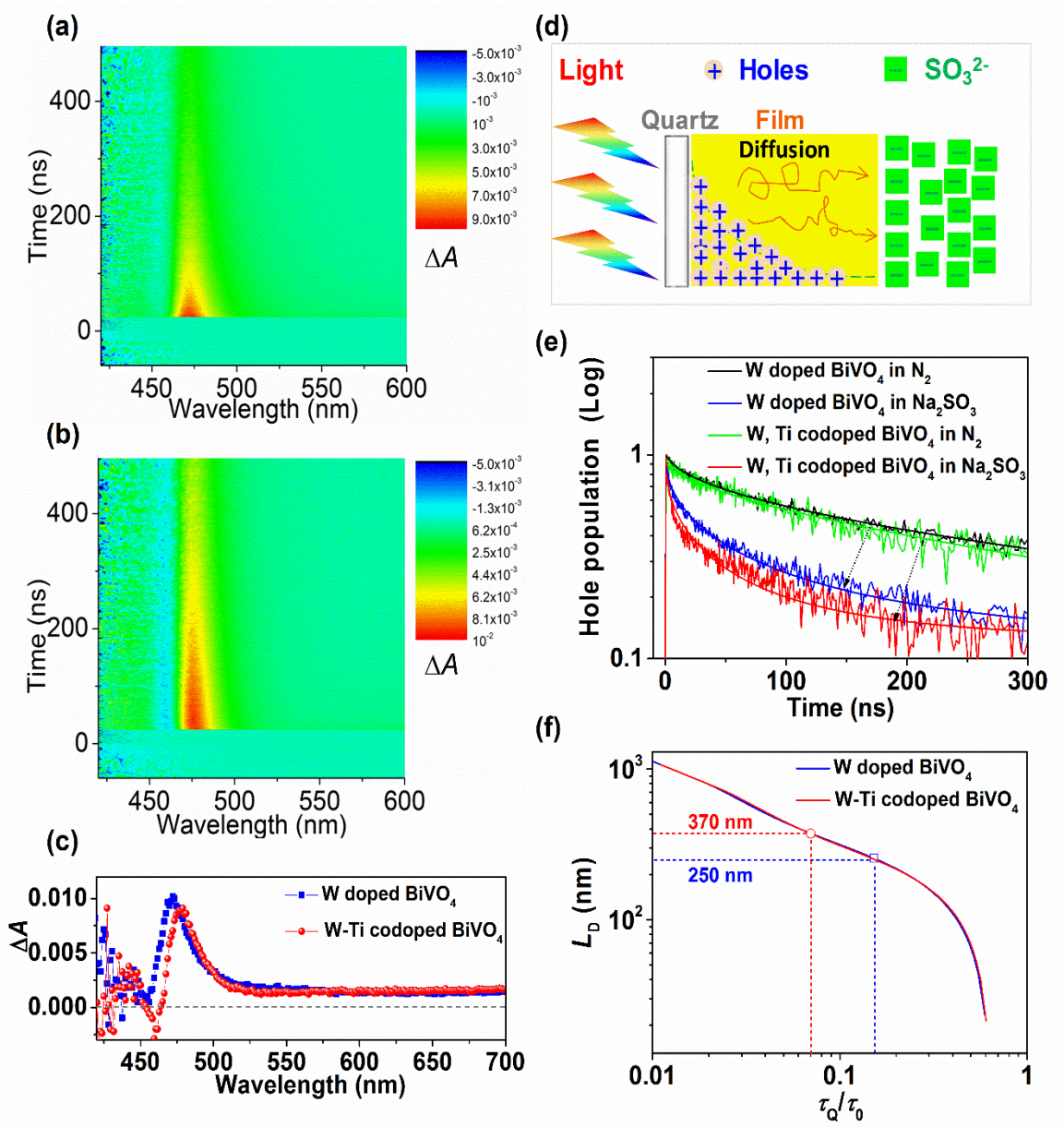

Fig. 3 The pseudo-color mappings of transient absorption profiles of (a) W doped and (b) W-Ti codoped $BiVO_4$ films (~170 nm) on quartz substrates. (c) Comparison of the transient absorption profiles of W doped and W-Ti codoped $BiVO_4$ films at selected delay time of around 1 ns. (d) Schematics of the optical mechanism to measure the hole diffusion length in $BiVO_4$ films. (e) The hole lifetimes obtained in transient absorption for W doped and W-Ti codoped $BiVO_4$ films with and without an efficient hole scavenger

Na_2SO_3. (f) The hole diffusion lengths of the W doped and W-Ti codoped $BiVO_4$ films obtained using the model depicted in the main text.

Fig. 3a-b shows the pseudo-color transient absorption profiles of W doped and W-Ti codoped $BiVO_4$ thin films. Fig. 3c shows the transient absorption profiles at selected delay time of around 1 ns. For W doped $BiVO_4$ film, a distinct positive peak ($\Delta A > 0$) can be seen at around 473 nm with a tail extending to beyond 700 nm, which are attributed to the photo-induced absorption (PIA) of the charge carriers (holes).[42] To evaluate the hole transport ability after the codoping, we setup a transient absorption experiment to measure the hole diffusion lengths in the W doped and W-Ti codoped films. The schematic of the experiment is shown in Fig. 3d which follows the standard procedures in measuring photovoltaic materials.[43, 44] In the experiment, a strong hole scavenger Na_2SO_3 solution is used to extract the holes.[45] The hole population follows the one-dimensional diffusion equation 3:

$$\frac{dN(z,t)}{dt} = D\frac{\partial^2 N(z,t)}{\partial z^2} + \frac{N(z,t)}{\tau} \tag{3}$$

where N is the hole density, z is the along the incident light direction (vertical to the film plane) with the quartz-$BiVO_4$ interface z=0 and $BiVO_4$-N_2 (or scavenger) interface z=L. D is the hole diffusion coefficient, and τ is the hole lifetime without any scavenger. Given a perfect scavenging of the holes at the interface, the boundary condition would be:

$$N(z,0) = N_0 \exp(-\alpha_L z); N(L,t) = 0 \tag{4}$$

where α_L is the absorption coefficient of the incident photon, L is the thickness of the film. The analytical solution of equation 3 with the boundary condition of equation 4 can be found elsewhere.[44] Fitting the hole decay dynamics with and without the hole scavenger will generate

the diffusion coefficient and the diffusion length of the holes. The hole absorption peak dynamics of the W doped and W-Ti codoped $BiVO_4$ are shown in Fig. 3e. The decay dynamics cannot be described by single exponential due to the involvement of multi-trapping and de-trapping of the charge carriers that usually occurs in oxides and organic semiconductors.[42, 46, 47] Here we simply use the effective lifetime (τ_{eff}) to represent the intrinsic hole lifetime τ_0, where τ_{eff} is the time that the carrier population drops to the 1/e of the maximum. The effective lifetime for the W doped $BiVO_4$ is around 276 ns, and drops to 229 ns for the W-Ti codoped film. With the hole scavenger Na_2SO_3, the effective lifetime of the W doped $BiVO_4$ drops to ~43 ns and that of the W-Ti codoped $BiVO_4$ decreases rapidly to ~16 ns due to the efficient hole extraction. It also indicates that the improved performance is not from a supposed longer lifetime; on the contrary, the lifetime decreases after the codoping. Further, hole diffusion length is investigated to understand the better performance by codoping. The concept of diffusion length based on Einstein relation can be used to evaluate the hole transport ability:

$$L_p = \sqrt{D_p \tau_p} \tag{5}$$

where D_p, τ_p are the hole diffusion coefficient and lifetime, respectively. According to the model in equation 3, such a decrease of lifetime with hole scavenger corresponds to a hole diffusion length of around 250 nm and 370 nm for the W doped and W-Ti codoped films, respectively, which are comparable to the values reported by others.[25, 48] Although these values derived from the equation may not be exactly the actual diffusion lengths due to various estimations made in the calculation, the comparison of the values can reflect the relative hole transport ability. The improvement of the diffusion length indicates that the codoping increases dramatically the hole mobility which facilitates its transport.

Table 1 Effective masses of electron and hole of pristine, W doped and W-Ti codoped $BiVO_4$.

	Effective mass of hole	Effective mass of electron
Pristine $BiVO_4$	0.837	0.459
W-doped $BiVO_4$	0.829	0.466
W-Ti codoped $BiVO_4$	0.840	0.482

In many metal oxides, carrier transport is expressed by a thermally activated small polaron hopping.[48, 49] If the phonon coupling is strong enough, the carrier transports by means of hopping. The phonon coupling coefficient α_{pc} is an indicator for the carrier transport. Usually, hopping happens at $\alpha_{pc} > 6$. And the coupling coefficient is related to effect mass in equation 6:

$$\alpha_{pc} \propto \left(m^*\right)^{1/2} \tag{6}$$

where, m* is the effective mass of carrier. As reported, the electrons transport by hopping in the $BiVO_4$ lattice (doped or undoped).[48, 50] We have calculated the effective masses of pristine, W doped and W-Ti codoped $BiVO_4$ (Fig. S13, and to calculate the effective mass electronic structure was calculated prior to the effective mass in Fig. S14). The effective masses of holes are relatively larger than those of electrons (Table 1). Hence, the coupling effect of hole and phonon is stronger than that of electron, which suggests the transport of hole is dominated by hopping. The mobility μ of polaron is expressed by:

$$\mu \propto \frac{1}{T}\exp\left(\frac{-W_H}{kT}\right) \tag{7}$$

where W_H is the polaron hopping activation energy, T is the temperature, and k is the Boltzmann's constant. The hopping activation energy W_H is given by

$$W_H \propto \frac{q^2}{4}\left(\frac{1}{\varepsilon_\infty} - \frac{1}{\varepsilon_0}\right) \tag{8}$$

where q is the hole charge, ε_∞ and ε_0 are the high frequency and static dielectric constant respectively. We calculated ε_∞, which remains the same for all of the three samples, at about 0.45. However, ε_0, is quite different: 4.1 for pristine $BiVO_4$, 146.3 for W doping, and 3.8 for W-Ti codoping. W doping causes an increase in the static dielectric constant, while W-Ti codoping lowers the value. Overall, the W_H is lowered by 11.5% after W-Ti codoping compared with mono W doping, which corresponds to the mobility increase by 29%.

3.3 Effect of W-Ti codoping on the surface catalysis

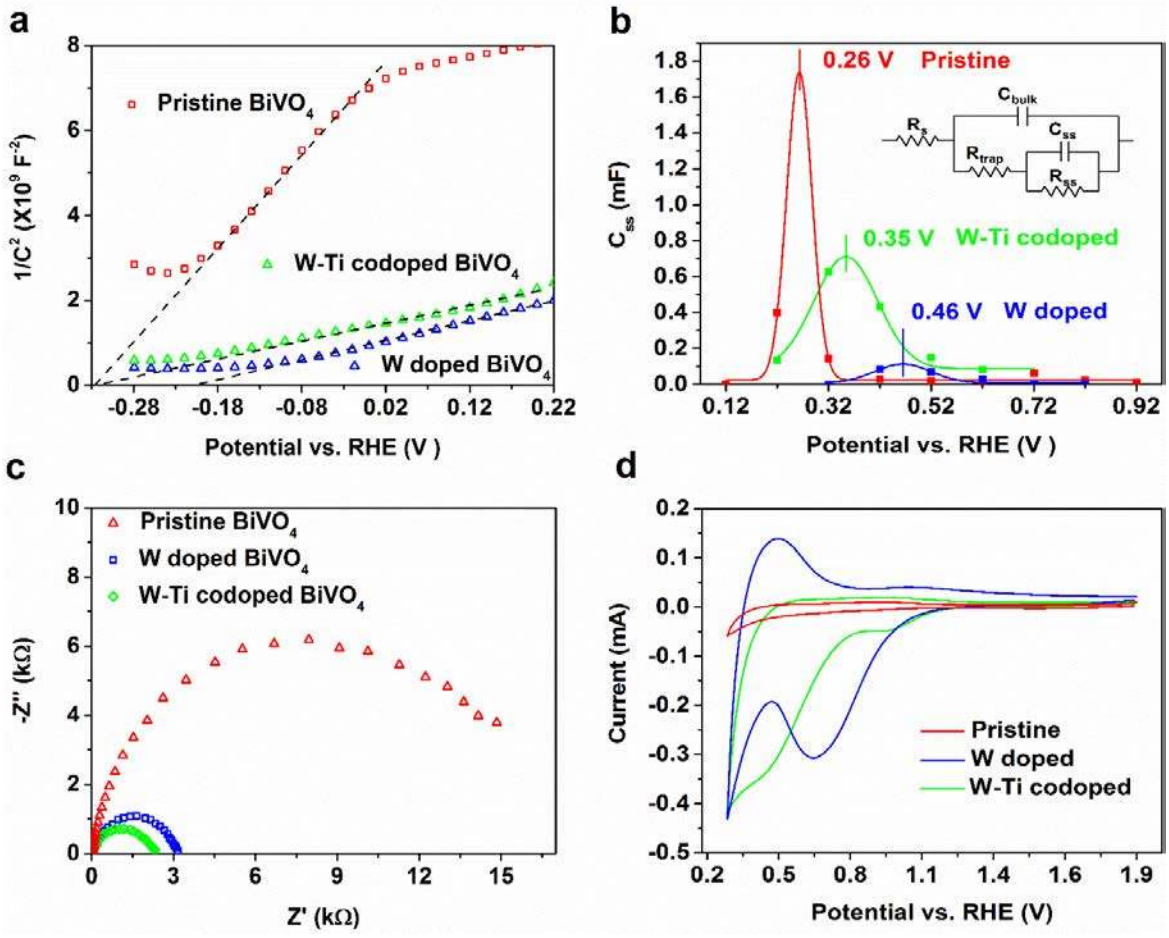

Fig. 4 (a) Mott-Schottky plots of pristine, W doped $BiVO_4$ and W-Ti codoped $BiVO_4$ at the frequency of 1 kHz in 0.5 M Na_2SO_4 aqueous solution. (b) C_{ss} determined from EIS (rectangle

points) measured under 1 sun illumination. Inset is the equivalent circuits employed to fit the experimental EIS data. (c) EIS of pristine, W doped and W-Ti codoped $BiVO_4$ photoelectrodes at the applied potential of 1.23 V_{RHE} under simulated solar illumination in 0.5 M Na_2SO_4 electrolyte. (d) Cyclic voltammetry scan of pristine, W doped and W-Ti codoped $BiVO_4$ in the dark in 0.5 M Na_2SO_4 electrolyte at a scan rate of 100 mV s^{-1} after holding the electrode at the potential of 1.8 V_{RHE} for 120 seconds under 1 sun illumination.

In Fig. 2a, another feature from codoping Ti is the photocurrent onset potential. Ti codoping causes a cathodic shift of photocurrent onset by 100 mV (0.68 V_{RHE} for W-Ti codoped $BiVO_4$ and 0.78 V_{RHE} for W doped $BiVO_4$). In order to understand this, experiments and theoretical calculation are conducted for further analyses.

Mott-Schottky plots are shown in Fig. 4a. The flat-band potential V_F of pristine $BiVO_4$ is estimated to be -0.32 V_{RHE}, while that of W doped $BiVO_4$ is about -0.20 V_{RHE}. There is a positive shift compared with pristine $BiVO_4$. However, after codoping with Ti, the flat-band potential is about -0.31 V_{RHE}, which is 0.11 V negative than that of W doped $BiVO_4$. This flat-band potential change correlates nicely with that of the photocurrent onset potential (0.1 V in Fig. 2a). The flat-band potential is generally considered to be located just under the conduction band of n-type semiconductors.[51] Thus, it is reasonable to deduce the shift of band potential corresponds to shift of the conduction band. Another feature caused by the W-Ti codoping is the carrier concentration change. From Mott-Schottky plots the carrier density is 1.2×10^{20} cm^{-3} for pristine $BiVO_4$, 4.46×10^{20} cm^{-3} for W-doped $BiVO_4$ and 4.89×10^{20} cm^{-3} for W-Ti codoped $BiVO_4$. W doping has increased the density greatly, while Ti codoping almost has no further enhancement

in the density. One would expect Ti to act as an acceptor as it has a valence state of 4^+, and thus compensates the extra electrons provided by W^{6+}. However, we find this is not true from the experiment, which could possibly be ascribed to the fact that the doping elements are at a low level and far separately from each other. Thus, W-doping and Ti-doping do not interfere with each other. Rather, they are able to improve electron and hole transport simultaneously.

It has been reported that the photocurrent onset is closely related with the charging of the surface states which generally exist on the metal oxide surfaces.[52] The open circuit potential also proves the existence of such surface states. In the dark, the equilibrium between the photoelectrode and the electrolyte dictates that the measured open-circuit potential reports on the position of the Fermi level.[53] Under ideal conditions, in the complete absence of an overpotential, an equilibrium open-circuit potential of 1.23 V would be expected, because the H_2O/O_2 redox couple dominates the electrochemical potential of the electrolyte in the dark. It was found that the equilibrium potential of pristine, W-doped and W-Ti codoped $BiVO_4$ were almost the same at around 0.61 V_{RHE} (Fig. S15), which was far below 1.23 V. Thus, it is supposed that there exist some surface states on the $BiVO_4$ surface. Equivalent circuit was employed here to analyze the photoelectrochemical processes.[54] In the equivalent circuit (inset in Fig. 4b), R_s represents total resistance from external circuit; R_{trap} represents the resistance of the surface states trapping holes; R_{ss} represents the surface charge transfer resistance from the surface states to oxidize water; C_{bulk} represents space charge capacitance of the bulk hematite; C_{ss} represents surface state capacitance, which dominates charging of the surface states, and have a close correlation with the photocurrent onset.[52] The C_{ss} of pristine, W doped, W-Ti codoped $BiVO_4$ obtained from EIS data is given in Fig. 4b. The values for C_{ss} show Gaussian behavior, and the charging potential follows the order of pristine < W-Ti codped < W doped. The charging potentials of C_{ss} somehow

also correlate with the photocurrent onsets except the pristine one, which is possibly due to poor conductivity and large resistance. Further discussion will be made next.

Fig. 4c shows the Nyquist plots of pristine, W doped and W-Ti codoped $BiVO_4$ at the applied potential of 1.23 V_{RHE}, which are used to study the surface charge injection at the interface. The same equivalent circuit (inset in Fig. 4b) was adapted for the analysis. The resistances of trapping holes by the surface states (R_{trap}) of pristine, W doped and W-Ti codoped $BiVO_4$ are 13320 Ω, 657 Ω and 35 Ω, respectively. Compared with doped $BiVO_4$, pristine one has a much larger hole trapping resistance, which requires a higher voltage to overcome the resistance. This explains why the pristine sample has a poor photocurrent onset, although it has a more negative conduction band and lower charging potential of the surface states in Fig. 4b. The surface charge transfer resistances R_{ss} of pristine, W doped and W-Ti codoped $BiVO_4$ are about 3996 Ω, 2272 Ω and 2218 Ω respectively. Thus, the doped samples have smaller charge transfer resistances than the pristine and W-Ti codoped $BiVO_4$. This tread agrees with the calculated charge transfer efficiencies. To unravel how W- Ti codoping affects the charge transfer, it is important to explore the surface condition in the $BiVO_4$. It is known that hydroxyterminated surface states will be formed on metal oxide electrode surface in aqueous solution.[52, 55-57] Thus, hole accumulation or trapping in these surface states can be treated as an oxidization process of these surface states, and thus these active surface states can be characterized cyclic voltammetry scan, in which current peak can be seen due to the reduction of those oxidized surface species.[57] To verify our speculation, we carried out cyclic voltammetry scan of $BiVO_4$ in Na_2SO_4 electrolyte at a scan rate of 100 $mV \cdot s^{-1}$ after holding the electrode at the potential of 1.8 V_{RHE} for 120 seconds under 1 sun illumination. Fig. 4d illustrates the changes on the surface states of $BiVO_4$ caused by mono W doping and W-Ti codoping compared with pristine one. For pristine $BiVO_4$, no obvious

reduction peak was observed. One obvious reduction current peak around 0.65 V_{RHE} emerged for the W doped sample. For W-Ti codoped sample, two obvious reduction peaks in the current around 1 V and 0.5 V_{RHE} were observed. These reduction current peaks are evidence of the surface states.[58] As seen, the W-Ti codoped sample have more active surface states to participate in the water oxidation, which implies that W-Ti codoping favors the surface catalysis.

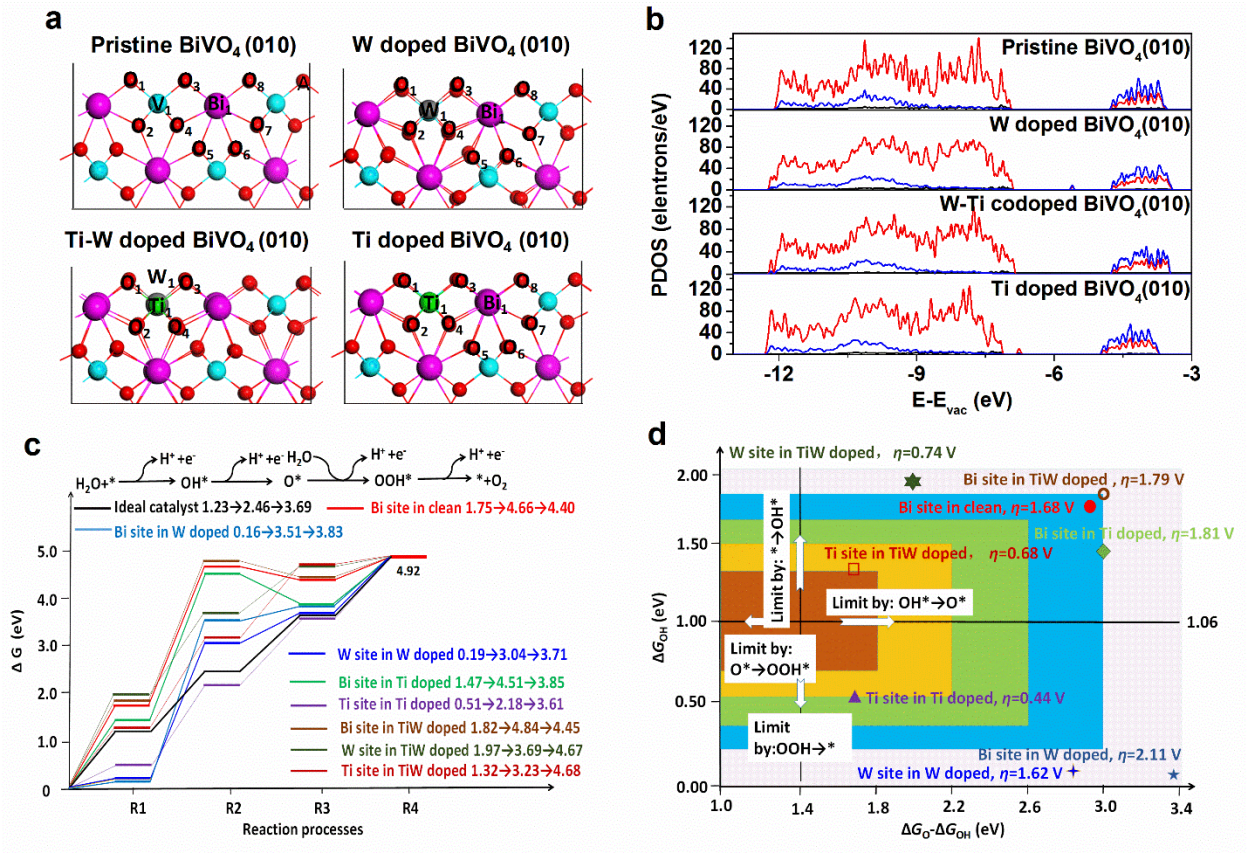

Fig. 5 (a) The optimized structures of Pristine, W doped, W-Ti codoped and Ti doped $BiVO_4$ (010) facet, where Bi, V, O, W and Ti showed as purple, gray, red, blue and green spheres, respectively. (b) The corresponding partial density of states (PDOS) of Pristine, W doped, W-Ti codoped and Ti doped $BiVO_4$ (010) facets. (c) Free-energy profiles of OER on different $BiVO_4$ surfaces, the black line is the ideal catalyst. The unit of Gibbs free energy is eV; (d) OER

theoretical overpotential (η) volcano where each region is labeled by the step limiting OER performance when the scaling relation between ΔG_{OH} and ΔG_{OOH} is $\Delta G_{OOH} = \Delta G_{OH} + 2.8$.

From Fig. 5a we can see that there are no obvious changes in the surface structure when doping W or Ti in the V site. However, from PDOS in Fig. 5b, it shows that mono doping on the surface will introduce unoccupied electronic states deep within the $BiVO_4$ bandgap, which is reported resulting from the donated electrons to form small electron polarons via self-trapping.[50] The deep level states are usually surface trap states, because α and β orbits in the deep level states are asymmetric (Fig. S16). Such trap states usually serve as recombination centers. However, no such kind of trap states are found in W-Ti codoped case, which indicates that W-Ti codoping facilitates the surface catalysis.

The calculated Gibbs free energies of five surface sites during OER process on $BiVO_4$ (010) surface are shown in Fig. 5c according to the adsorption of several key species (Fig. S17), which shows different ability for water splitting. Comparing the Gibbs free energy on different sites, it is found the Ti site is closer to ideal OER catalysis process than other sites, indicating that Ti site is energetically more favorable for water splitting. In order to further understand the surface catalytic ability, the overpotentials of different surface sites were also calculated, as shown in Fig. 5d. Compared with pristine $BiVO_4$, no much improvement has been found on the overpotential in Bi or W site. However, Ti site possesses a lower overpotential in W-Ti codoped sample (0.68 V). This well explains the observed photocurrent onset potential shift in W-Ti codoped $BiVO_4$. Although Ti site on Ti doped surface also shows a low overpotential (0.44 V), the experimentally observed performance was poor. This is mainly due to the fact that Ti mono doped sample has poor electron conductivity and consumes more voltage to overcome the large resistance, which

again proves that Ti doping can only become effective after the poor electron transport has been solved by W doping.

4. Conclusions

Quantitative analysis shows that the low charge separation (22%) is the limiting factor for the poor performance of pristine $BiVO_4$. W doping, which improves the electron conductivity, enhances the charge separation from 22% to 42% (at 1.23 V_{RHE}). However, the photocurrent of W doped $BiVO_4$ is far below the theoretical value. In this study, we find W-Ti cooping enhances the photocurrent to about 2 times the one of W mono-doping, while Ti mono-doping has nearly no effect on the photocurrent improvement. This enhancement is mainly attributed to the better charge separation efficiency (79% at 1.23 V_{RHE}). Further, the enhanced charge separation is found to arise from the enhanced hole transport. Transient absorption spectroscopy shows that the hole diffusion length of W doped $BiVO_4$ is around 250 nm, and it increases to around 370 nm for the W-Ti codoped $BiVO_4$. The improvement of the hole diffusion length indicates that the W-Ti codoping increases dramatically the hole mobility which facilitates its transport. Theoretical results show that W doping increases the static dielectric constant which lowers the carrier mobility. W-Ti codoping lowers the static dielectric constant, thus, the hole polaron hopping activation energy W_H is lowered by 11.5% after W-Ti codoping. Moreover, W-Ti codoping causes a cathodic shift of photocurrent onset potential by 100 mV compared with W doped $BiVO_4$. The calculated adsorption energy and reaction Gibbs free energies indicate that Ti site is energetically more favorable for water splitting. Moreover, Ti site possesses a lower overpotential in W-Ti codoped sample (0.68 V) compared with mono W doped sample (1.68 V). The current study sheds light onto ways to identify the key factor(s) and to improve the charge separation and transfer efficiencies of a compact photoelectrode. It indicates that in a photo

electrode system, the minority carrier mobility is also an important consideration. High solar conversion efficiency can only be obtained under a well-balanced electron and hole transport system.

Conflicts of interest

The authors declare no competing financial interests.

Author contributions

†X.Z. and J.H contributed equally to this work.

X.Z., S.C. T.C.S. and Z.C. conceived and directed the project. X.Z. developed the concept and carried out the sample preparation, most characteration and PEC performance experiments and data analysis. J.H. contributed the theoretical calculation on the surface catalysis and most discussion on the mechanism. B.W. contributed to the investigation of the photophysics and carrier dynamics in the W doped and W-Ti co-doped $BiVO_4$ films and data analysis. J.F. contributed to the discussion of performance enhancement by codoping and light absorption analysis. Z. Z. contributed the discussion on the polaron hopping mechanism and help the calculation of the dielectric constant. A.B. and R.A. contributed to the theoretical calculations and data analysis. S.C. contributed to the XPS experiment and data analysis.

Acknowledgements

Great thanks to Daming Zhao (PHD candidate from School of Physical and Mathematical Sciences, Nanyang Technological University) for the discussion of the hole transport mechanism. Financial supports from Ministry of Education (grant RG15/16). Financial supports from Nanyang Technological University in form of SUG.C Singapore National Research Foundation through the Singapore-Berkeley Initiative for Sustainable Energy (SINBERISE) CREATE Programme. The National Natural Science Foundation of China (No. 21676216). Financial

supports from Erusmus Mundus, Swedish Research Council (VR), Swedish Energy Agency are gratefully acknowledged.

References

1. A. J. Heeger, *Chem. Soc. Rev.,* 2010, **39**, 2354-2371.

2. M. Liu, M. B. Johnston and H. J. Snaith, *Nature,* 2013, **501**, 395-398.

3. Z. Li, W. Luo, M. Zhang, J. Feng and Z. Zou, *Energy Environ. Sci.,* 2013, **6**, 347-370.

4. T. Hisatomi, J. Kubota and K. Domen, *Chem. Soc. Rev.,* 2014, **43**, 7520-7535.

5. N. T. Hahn and C. B. Mullins, *Chem. Mater.,* 2010, **22**, 6474-6482.

6. W. Luo, Z. Yang, Z. Li, J. Zhang, J. Liu, Z. Zhao, Z. Wang, S. Yan, T. Yu and Z. Zou, *Energ y Environ. Sci.,* 2011, **4**, 4046-4051.

7. Q. Dong, Y. Fang, Y. Shao, P. Mulligan, J. Qiu, L. Cao and J. Huang, *Science,* 2015, **347**, 96 7-970.

8. C. Santato, M. Odziemkowski, M. Ulmann and J. Augustynski, *J. Am. Chem. Soc.,* 2001, **123**, 10639-10649.

9. M. D. Kelzenberg, S. W. Boettcher, J. A. Petykiewicz, D. B. Turner-Evans, M. C. Putnam, E. L. Warren, J. M. Spurgeon, R. M. Briggs, N. S. Lewis and H. A. Atwater, *Nat. Mater.,* 2010, **9**, 239-244.

10. X. Zhao, W. Luo, J. Feng, M. Li, Z. Li, T. Yu and Z. Zou, *Adv. Energy Mater.,* 2014, **4**, 1301 785.

11. A. Kay, I. Cesar and M. Grätzel, *J. Am. Chem. Soc.* 2006, **128**, 15714-15721.

12. Z. Li, J. Feng, S. Yan and Z. Zou, *Nano Today* 2015, **10**, 468-486.

13. P. M. Rao, L. Cai, C. Liu, I. S. Cho, C. H. Lee, J. M. Weisse, P. Yang and X. Zheng, *Nano L ett.,* 2014, **14**, 1099-1105.

14. M. G. Ahmed, T. A. Kandiel, A. Y. Ahmed, I. Kretschmer, F. Rashwan and D. Bahnemann, *J. Phys. Chem. C,* 2015, **119**, 5864-5871.

15. Z. Yang, B. Chang, J. Zou, J. Qiao, P. Gao, Y. Zeng and H. Li, *Appl. Optics,* 2007, **46,** 7035-7039.

16. F. F. Abdi, L. Han, A. H. Smets, M. Zeman, B. Dam and R. van de Krol, *Nat. Commun.*, 201 3, **4**, 2195.

17. Y. Yang, M. Forster, Y. Ling, G. Wang, T. Zhai, Y. Tong, A. J. Cowan and Y. Li, *Angew. Ch em. Int. Ed.,* 2016, **55**, 3403-3407.

18. W. Luo, Z. Li, T. Yu and Z. Zou, *J. Phys. Chem. C,* 2012, **116**, 5076-5081.

19. D. Cao, W. Luo, J. Feng, X. Zhao, Z. Li and Z. Zou, *Energy Environ. Sci.,* 2014, **7**, 752-759.

20.F. Le Formal, N. Tétreault, M. Cornuz, T. Moehl, M. Grätzel and K. Sivula, *Chem. Sci.,* 2011, **2**, 737-743.

21. L. Steier, I. Herraiz-Cardona, S. Gimenez, F. Fabregat-Santiago, J. Bisquert, S. D. Tilley and M. Grätzel, *Adv. Funct. Mater.,* 2014, **24**, 7681-7688.

22. T. Hisatomi, F. Le Formal, M. Cornuz, J. Brillet, N. Tétreault, K. Sivula and M. Grätzel, *Ene rgy Environ. Sci.,* 2011, **4**, 2512-2515.

23. Y. Liu, Y. Jiang, F. Li, F. Yu, W. Jiang and L. Xia, *J. Mater. Chem. A*, 2018, **DOI:**10.1039/C 8TA01304G.

24. Y. Hu, Y. Wu, J. Feng, H. Huang, C. Zhang, Q. Qian, T. Fang, J. Xu, P. Wang and Z. Li, *J. Mater. Chem. A*, 2018, **6**, 2568–2576.

25. D. K. Zhong, S. Choi and D. R. Gamelin, *J. Am. Chem. Soc.,* 2011, **133**, 18370-18377.

26. M. Li, W. Luo, D. Cao, X. Zhao, Z. Li, T. Yu and Z. Zou, *Angew. Chem. Int. Ed.,* 2013, **52**, 1 1016-11020.

27. I. S. Cho, C. H. Lee, Y. Feng, M. Logar, P. M. Rao, L. Cai, D. R. Kim, R. Sinclair and X. Zh eng, *Nat. Commun.*, 2013, **4**, 1723.

28. Y. Gai, J. Li, S.-S. Li, J.-B. Xia and S.-H. Wei, *Phys. Rev. Lett.*, 2009, **102**, 036402.

29. Z. Jiao, J. Zheng, C. Feng, Z. Wang, X. Wang, G. Lu and Y. Bi, *ChemSusChem*, 2016, **9**, 282 4-2831.

30. T. Morikawa, T. Arai and T. Motohiro, *Appl. Phys. Express*, 2013, **6**, 041201.

31. W.-J. Yin, H. Tang, S.-H. Wei, M. M. Al-Jassim, J. Turner and Y. Yan, *Phys. Rev. B*, 2010, **82**, 045106.

32. T. W. Kim and K.-S. Choi, *Science,* 2014, **343**, 990-994.

33. J. Hu, W. Chen, X. Zhao, H. Su and Z. Chen, *ACS Appl. Mater. Inter.*, 2018, **10**, 5475-5484.

34. W. Luo, J. Wang, X. Zhao, Z. Zhao, Z. Li and Z. Zou, *Phys. Chem. Chem. Phys.,* 2013, **15**, 1006-1013.

35. F. F. Abdi, N. Firet and R. van de Krol, *ChemCatChem,* 2013, **5**, 490-496.

36. S. J. Hong, S. Lee, J. S. Jang and J. S. Lee, *Energy Environ. Sci.*, 2011, **4**, 1781-1787.

37. M. Li, L. Zhao and L. Guo, *Int. J. Hydrogen Energy*, 2010, **35**, 7127-7133.

38. S. Ho-Kimura, S. J. Moniz, A. D. Handoko and J. Tang, *J. Mater. Chem. A*, 2014, **2**, 3948-3953.

39.H. Dotan, K. Sivula, M. Grätzel, A. Rothschild and S. C. Warren, *Energy Environ. Sci.,* 2011, **4**, 958-964.

40. X. Zhao and Z. Chen, *Beilstein J. Nanotech.,* 2017, **8**, 2640-2647.

41. X. Yao, D. Wang, X. Zhao, S. Ma, P. S. Bassi, G. Yang, W. Chen, Z. Chen and T. Sritharan, *Energy Technol.,* 2018, **6**, 100-109.

42. J. Ravensbergen, F. F. Abdi, J. H. van Santen, R. N. Frese, B. Dam, R. van de Krol and J. T. Kennis, *J. Phys. Chem. C,* 2014, **118**, 27793-27800.

43. B. Wu, H. T. Nguyen, Z. Ku, G. Han, D. Giovanni, N. Mathews, H. J. Fan and T. C. Sum, *Adv. Energy Mater.,* 2016, **6**, 1600551.

44. G. Xing, N. Mathews, S. Sun, S. S. Lim, Y. M. Lam, M. Grätzel, S. Mhaisalkar and T. C. Sum, *Science,* 2013, **342**, 344-347.

45. Y. Ma, S. R. Pendlebury, A. Reynal, F. Le Formal and J. R. Durrant, *Chem. Sci.,* 2014, **5**, 2964-2973.

46. X. Wang, Z. Feng, J. Shi, G. Jia, S. Shen, J. Zhou and C. Li, *Phys. Chem. Chem. Phys.,* 2010, **12**, 7083-7090.

47. J. Guo, H. Ohkita, S. Yokoya, H. Benten and S. Ito, *J. Am. Chem. Soc.,* 2010, **132**, 9631-9637.

48. A. J. Rettie, H. C. Lee, L. G. Marshall, J.-F. Lin, C. Capan, J. Lindemuth, J. S. McCloy, J. Zh ou, A. J. Bard and C. B. Mullins, *J. Am. Chem. Soc.,* 2013, **135**, 11389-11396.

49. N. F. Mott and E. A. Davis, *Electronic processes in non-crystalline materials*, OUP Oxford, 2012.

50. T. W. Kim, Y. Ping, G. A. Galli and K.-S. Choi, *Nat. Commun.,* 2015, **6**, 8769.

51. K. Sayama, A. Nomura, T. Arai, T. Sugita, R. Abe, M. Yanagida, T. Oi, Y. Iwasaki, Y. Abe and H. Sugihara, *J. Phys. Chem. B,* 2006, **110**, 11352-11360.

52. B. Klahr, S. Gimenez, F. Fabregat-Santiago, T. Hamann and J. Bisquert, *J. Am. Chem. Soc.,* 2012, **134**, 4294-4302.

53. C. Du, X. Yang, M. T. Mayer, H. Hoyt, J. Xie, G. McMahon, G. Bischoping and D. Wang, *A ngew. Chem. Int. Ed.,* 2013, **52**, 12692-12695.

54. B. Klahr and T. Hamann, *J. Phys. Chem. C,* 2014, **118**, 10393-10399.

55. P. Salvador, *J. Electrochem. Soc.,* 1981, **128**, 1895-1900.

56.B. E. Conway and B. V. Tilak, in *Advances in Catalysis*, eds. H. P. D.D. Eley and B. W. Paul, Academic Press, 1992, vol. Volume 38, pp. 1-147.

57. X. Zhao, J. Feng, S. Chen, Y. Huang, T. C. Sum and Z. Chen, *Phys. Chem. Chem. Phys.,* 201 6, **19**, 1074-1082.

58. B. Klahr, S. Gimenez, F. Fabregat-Santiago, J. Bisquert and T. W. Hamann, *Energy Environ. Sci.,* 2012, **5**, 7626-7636.